ULTRASONIC EVALUATION OF WEAK LINER/PROPELLANT BONDING IN A ROCKET MOTOR

A. N. Sinclair[1], M. Jastrzebski[1], and V. Safavi-Ardebili[1]
[1] Department of Mechanical and Industrial Eng., University of Toronto, Canada

Abstract: An attempt was made to develop an ultrasonic nondestructive evaluation technique for detection of poor interfacial bonding between the rubber liner of a cylindrical rocket motor and the solid fuel propellant. The challenge originates from the very poor ultrasonic transmission properties of the rubber liner, and also from the acoustic impedance mismatch between the rubber and outer steel casing of the structure.

Experiments were conducted to investigate the feasibility of using various ultrasonic techniques to characterize the bond condition. Attenuation of the rubber liner layer was assessed for both compression and shear modes using the Kramers-Kronig relationships to derive attenuation coefficients from dispersion curves; these showed the impracticality of guided modes for this test subject due to the enormous shear attenuation coefficient at frequencies above 500 kHz.

Normal beam compression and shear wave testing was performed on various areas of a simulated rocket motor, which had been manufactured with implanted defects at marked locations on the casing as well as flat specimens with well-defined defect types. It was possible to distinguish between the "good" areas and the areas labeled as "debond rubber" and "debond steel". These differences were clearly visible using compression waves at 5 MHz. The differences were very small and variable using 250 kHz shear waves, and generally visible only in the frequency domain.

Although total debonds are detectable by this technique, no definite conclusion can be drawn regarding the detection of "kissing bonds", as the condition of the bond at the "damaged" areas of the simulated motor was unknown.

Introduction: This project is focused on the detection and characterization of weak interfacial bonding between two layers of a cylindrical AIM-9 air-to-air missile, consisting of an outer steel casing, rubber liner, and inner core of solid propellant. The solid propellant rocket motor used in the AIM-9 air-to-air missile is a cylindrical structure consisting of a steel outer sleeve, thin rubber liner and polymer propellant core (Figure 1). This structure is susceptible to weak bonding between the rubber liner and the propellant. Artificial debonds have been manufactured in one test sample by deliberately placing a patch of silicone grease at the interface during the manufacturing process. It has been proposed that the weak bond might be detected and located using leaky Lamb waves that would propagate along the steel/rubber structure.

Figure 1: Solid Rocket Motor Cross-section

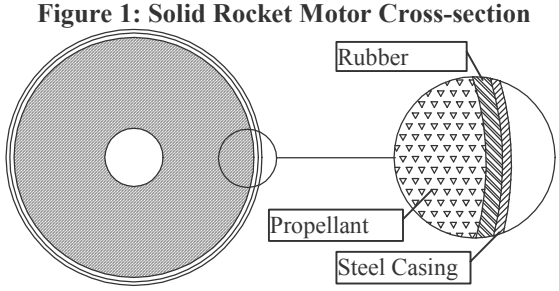

The properties of the rubber are crucial to the proposed inspection method. Lamb waves contain a strong shear component, but some types of rubber have enormous attenuation coefficients for shear waves. The large impedance mismatch between the rubber and steel will also impede the transfer of acoustic energy between these two materials, thereby making it more difficult to interrogate the rubber/propellant boundary. Also of interest to this investigation is the extent of acoustic impedance mismatch between the rubber and propellant; if the mismatch is very small, then it may be easier to detect a sudden jump in the mismatch originating form a partial debond. The extent of rubber/propellant impedance mismatch will also have implications regarding the confinement of the Lamb wave to the steel and rubber liner layers of the system.

The classical equations for guided waves traveling in a single or multi-layered plate were reported by Viktorov [1] and Brekhovskikh [2]. Their original formulation ignored attenuation effects, although they could be incorporated within a first-order approximation by using complex values for the shear and longitudinal wavenumbers k. Many researchers used these equations as a means to measure properties such as the elastic moduli, e.g., [3]. It was also noted that the boundary conditions on the plate could affect the frequencies of the various propagation modes or their damping coefficients [4].

A similar challenge was faced by researchers studying guided waves traveling in a two-layered plate consisting of a steel or aluminum adherend plus a layer of adhesive, e.g., [5] and [6]. Cawley [7] and Guy et al [8] noted that most of the energy was concentrated in the metal adherend rather than the adhesive, such that the ultrasonic signatures had minimal sensitivity to changes in the adhesive thickness or its mechanical properties. This has grave implications for our project, as we would require significant ultrasonic energy to propagate in the rubber if there is to be sensitivity to the bond condition at the rubber/propellant interface.

In general, the above researchers were concentrating on-2-layered structures, where the bond of interest links the two layers. Our case is somewhat unique, in that the bond between the steel casing and rubber is not our target, rather it is the boundary condition between the rubber liner and propellant on the far (inaccessible) side of the target. Only a small number of publications deal with this type of configuration.

A low-frequency air-coupled transmission method [9] was applied to the inspection of large solid-propellant rocket motors. This method relies on the use of very low frequency ultrasound (50-60 kHz) to overcome the high signal attenuation caused by thick layers of rubber insulation and propellant in their test configuration. Unfortunately, the physical dimensions of the AIM-9 rocket motor make it unfeasible to use such low frequencies.

NASA has been working on a closely related problem on a solid rocket motor, with possible application to their shuttle program. Due to the thin layer thicknesses, they faced difficulties in resolving multiple echoes in a conventional normal-beam pulse-echo inspection. Their solution was to use normal-beam compression waves, and monitor the attenuation of the returned echoes, plus the frequencies of the resonant modes in the Fourier domain. Their configuration was somewhat different from ours in that they had to contend with a four-layered structure, but all layers were reasonably efficient transmitters of ultrasound. They were successful in seeing changes in the response spectrum when there was complete delamination between two layers in their system [10].

The selection of an ultrasonic inspection method for this scenario is strongly governed by the degree to which it is able to overcome the above difficulties. It is therefore crucial that the mechanical properties of the constituent layers be quantified beforehand, so that an optimal design of the inspection system can be developed. It was decided to proceed first with the characterization of the acoustic properties of the rubber liner, namely the velocity and attenuation factor for compressional and shear waves.

One method of phase velocity measurement in dispersive media, as suggested by [11], is by phase spectrum comparison. The method relies on computing the phase spectra of a signal transmitted through the specimen, and a reference signal using separate transducers as transmitter and receiver. The reference signal is obtained by placing the two transducers in direct contact with each other. The difference between the phase spectra of the reference signal and through-transmitted pulse can be related to the phase velocity by the following equation:

Equation 1
$$c_p(\omega) = \frac{\omega L}{\left(\phi(\omega) - \phi_o(\omega)\right)}$$

where , c_p is the phase velocity, ω is the angular frequency, L is the specimen thickness, ϕ is the through-transmitted phase spectrum, and ϕ_0 is the reference phase spectrum. Equation 1

yields the phase-velocity as a function of frequency, over the range of frequencies common to both the reference and through-transmitted signals.

Wave dispersion is closely linked to wave attenuation. The attenuation characteristics of a material can be determined through direct measurement or from the Kramers-Kronig relationship [12]-[14]. The latter show that attenuation is related to phase velocity according to:

Equation 2
$$\alpha(\omega) = \frac{\pi\omega^2}{2c_p{}^2(\omega)} \frac{dc_p(\omega)}{d\omega}$$

where, α is the attenuation factor, and c_p is the phase velocity. The great advantage of this technique is that ultrasonic velocity measurements can usually be made far more accurately than direct attenuation measurements. Equation 2 then allows us to derive the attenuation spectrum from velocity measurements [14].

The measurement technique chosen was based on the method proposed by [11]; however, it was modified for compression waves to function in an immersed through-transmission setup. For compression velocity measurements, the setup consists of a water-filled immersion tank with two transducers positioned to face each other. One transducer functions as the emitter or transmitter (ET) and the other as the receiver (RT). The sample can be inserted or removed from the path of the ultrasonic beam traveling from ET to RT (Figure 2).

Figure 2: Schematic Diagram of Immersion Setup

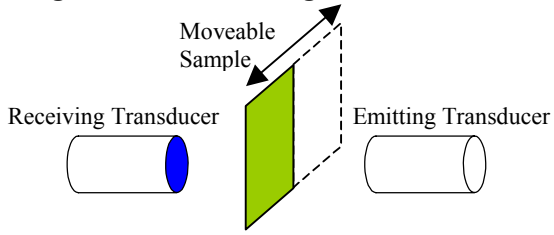

Assuming that the attenuation coefficient of water is negligible, one can use Equation 1 to obtain Equation 3 for the immersion test configuration as described above:

Equation 3
$$c_{p,ls}(\omega) = \left(\frac{\frac{\phi(\omega) - \phi_o(\omega)}{\omega}}{d_s} + \frac{1}{c_{p,lw}} \right)^{-1}$$

where, d_s is the sample thickness, $c_{p,lw}$ is the phase velocity of longitudinal waves in water, ϕ is the through-transmitted phase spectrum with the sample in place, and ϕ_0 is the reference phase spectrum with the sample removed. Equation 3 gives the phase velocity as a function of frequency, provided that the phase spectra of signals with and without the sample inserted are known. These spectra can be easily obtained using Fast Fourier Transforms of recorded signals.

Once the velocity spectrum has been determined, it is possible to calculate the compressional wave attenuation coefficient as a function of frequency from Equation 2. It is also possible to estimate this compressional wave attenuation coefficient directly from amplitude measurements made in the immersion setup. In comparison to rubber, the attenuation coefficient of water in the low MHz range is negligible. Therefore, the absolute attenuation coefficient of the rubber sample from the amplitude spectra of the signals is approximately:

Equation 4
$$\alpha(\omega) = \frac{20}{d_s} \log\left(\frac{A_s(\omega)}{A_w(\omega)} \right)$$

where, A_s is the amplitude spectrum with the sample inserted in the beam path, and A_w is the amplitude spectrum with the sample removed from the beam path.

The method described above is not applicable to shear velocity measurement, as water is incapable of sustaining shear stresses. The method was modified to find the difference between the phase spectra of signals transmitted through two samples of different thickness in a contact test configuration. The transducers in this case must be adequately coupled to allow shear waves to pass in and out of the samples. One could show that the phase velocity of shear waves can be obtained from:

Equation 5

$$c_{p,ss}(\omega) = \frac{\omega \Delta d}{\phi(\omega) - \phi_o(\omega)}$$

where, Δd is the difference between the thicknesses of the two samples.

The normal-beam, shear transducers were coupled directly to both sides of the rubber samples using phenyl salicylate (Salol), an organic salt with a melting point of 43°C. As described above, the technique required at least two specimens of different thickness. Since the sample liner material was available only in thin, uniform thickness sheets, it was necessary to construct thick samples. These were prepared by adhering together multiple sheets with an extremely thin layer of commercial contact cement.

Results: The density of the rubber was determined by measuring the mass and volume of the rubber sample. These measurements yielded a value of 1706 kg/m^3. The material impedance to shear or compression waves could now be determined by multiplying the density by the shear or compression wave speed, at the frequency of interest.

The longitudinal velocity measurements for three different probes showed a high level of consistency in the frequency ranges where overlap between transducer spectra occurred (Figure 3-A). It was found that uncertainty in the individual measurements increased away from the central frequency. This is expected, as only a small fraction of the total energy is emitted and received at the extreme edges of the transducer frequency spectrum, and the measurements are therefore more sensitive to noise in these regions.

Figure 3: (A) Longitudinal Phase Velocity in Rubber Liner, as Measured with Three Transducers. (B) Longitudinal Attenuation Coefficient in Rubber Liner, Measured and Calculated Using Eq. 2

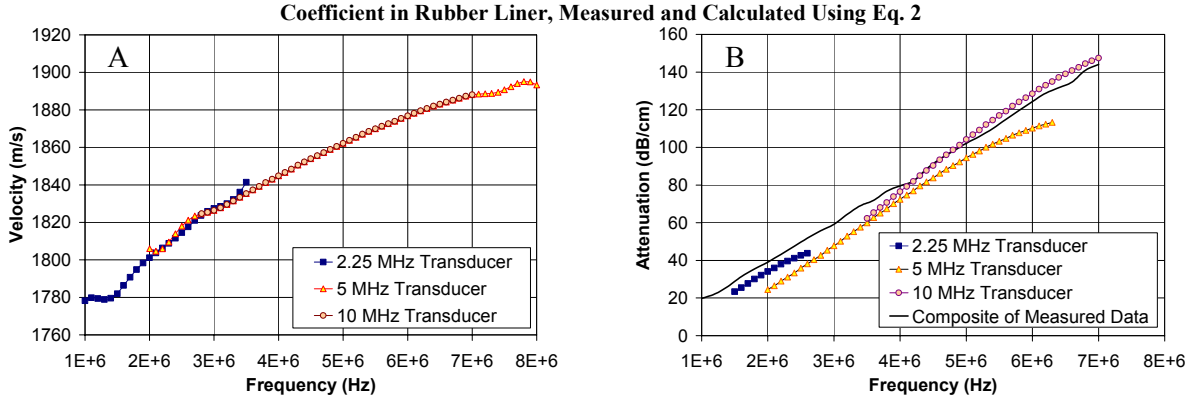

A measurable increase in compression wave velocity was observed with increasing frequency, going from 1800 m/s at 2 MHz to almost 1900 m/s at 8 MHz. As seen for other viscoelastic materials, the velocity does tend to level off at high frequencies where relaxation effects play a diminishing role.

Figure 3-B shows the longitudinal wave attenuation coefficient as a function of frequency. Both direct amplitude measurements according to Equation 4, and values obtained from the Kramers-Kronig relationship of Equation 2, are plotted. The direct measurements showed a great deal of overlap and are hence grouped into a single "composite" data set. The data curves derived from the Kramers-Kronig relationship for each transducer are shown separately; they do not show perfect agreement, although the discrepancies are sufficiently small that an approximate value for the attenuation coefficient can be obtained within the relevant frequency range. The compression wave attenuation coefficient ranges from about 25 db/cm at 2 MHz to 125 db/cm at 6 MHz.

Figure 4-A shows the experimental phase velocity versus frequency plot for a shear wave propagating in the rubber liner material. Shear velocities range from only 300 m/s at 100 kHz to 1000 m/s at 700 kHz. The contrast in the quality of the data between this and the longitudinal wave measurements is clear. It is also apparent that the shear phase velocity increases much more steeply with increasing frequency than it does for longitudinal waves, indicating much stronger attenuation.

Figure 4: (A) Measured Phase Velocity of Shear Wave vs. Frequency in Rubber Liner. (B) Shear Attenuation Coefficient vs. Frequency in Rubber Liner.

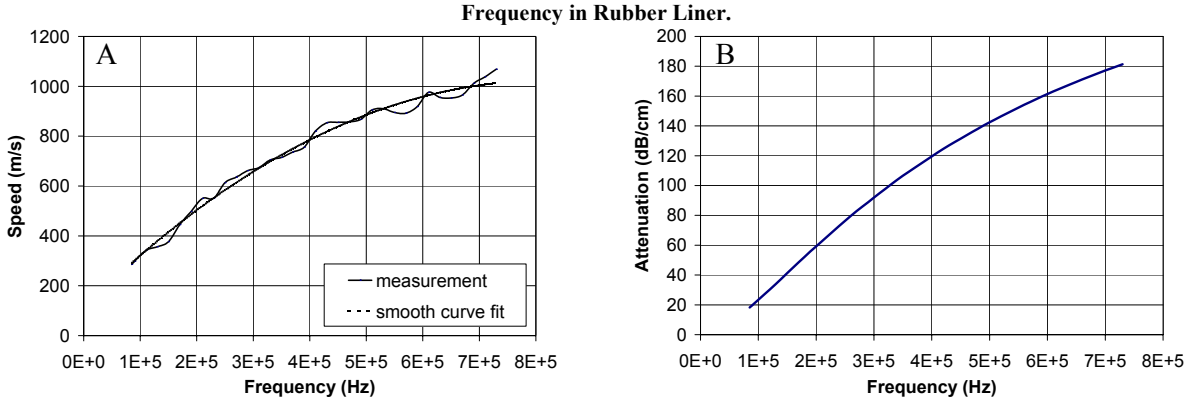

For estimates of the shear wave attenuation, amplitude measurements are extremely inaccurate. This is because of difficulties in obtaining repeatable coupling efficiencies between the transducers and sample, even with the use of Salol. Because of the practical complications, the shear attenuation coefficient is presented only as determined from the Kramers-Kronig relationship in Figure 4-B. Due to the significant noise in the velocity data and the difficulty in fitting an appropriate curve, it is clear that the accuracy of the shear attenuation coefficient will be somewhat lower than that obtained for the longitudinal attenuation coefficient.

The results nonetheless show that the shear attenuation coefficient increases much more sharply than the longitudinal attenuation coefficient. At frequencies above 350 kHz the rubber has a shear attenuation coefficient of over 100dB/cm. A comparison of the shear and longitudinal attenuation curves indicates that shear attenuation near 1MHz is above 200 dB/cm - about 20 times the value for compression waves.

With the acoustic properties of the liner in hand, it is possible to analyze the degree of acoustic impedance mismatch and returned signal strength for various bond conditions. Acoustic properties for the rubber liner are those obtained experimentally in this work, with the properties for the remaining materials being those tabulated in the separate studies [15], [16]. A plot of the estimated returned signal strength vs. frequency for a longitudinal wave normally incident on the rocket casing is shown in Figure 5-A. The graph shows signal losses due to attenuation plus impedance mismatch at the rubber/steel interface. It is assumed that perfect coupling exists between the transducer and the casing, and that "good" bonds between layers are perfect. By contrast, debonds are approximated by a layer of air resulting in 100% reflection at the interface. A kissing bond would lie somewhere between these two extremes. Three cases are shown:

(1) The echo from the rubber/casing interface. The loss is close to 0 dB at all frequencies, forming a horizontal line near the top of the graph. This is because there is almost 90% reflection from the interface, due to the large impedance mismatch.

(2) The echo from the rubber/propellant interface assuming that it is completely debonded. There is substantial signal loss due to both attenuation in the rubber, and poor signal transmission across the steel/rubber boundary. The losses are only 20 dB at 1 MHz, but 80 dB at 9 MHz.

(3) The echo from the rubber/propellant interface, assuming that the interface is a perfect bond. In this case, a substantial amount of the ultrasonic energy reaching the rubber/propellant interface will go into the propellant, resulting in an echo signal that is about 20 dB weaker than in case 2.

A corresponding plot for an incident shear wave is shown in Figure 5-B; however, the frequency range is much lower. Due to a lack of data regarding shear impedance of the propellant material, one cannot compute the shear reflection coefficient from a well-bonded rubber/propellant interface. In fact, both the rubber and propellant are extremely poor conductors of shear waves.

Figure 5: (A) Calculated Drop in Echo Amplitude vs. Frequency, Longitudinal Wave. (B) Calculated Drop in Echo Amplitude vs. Frequency, Shear Wave.

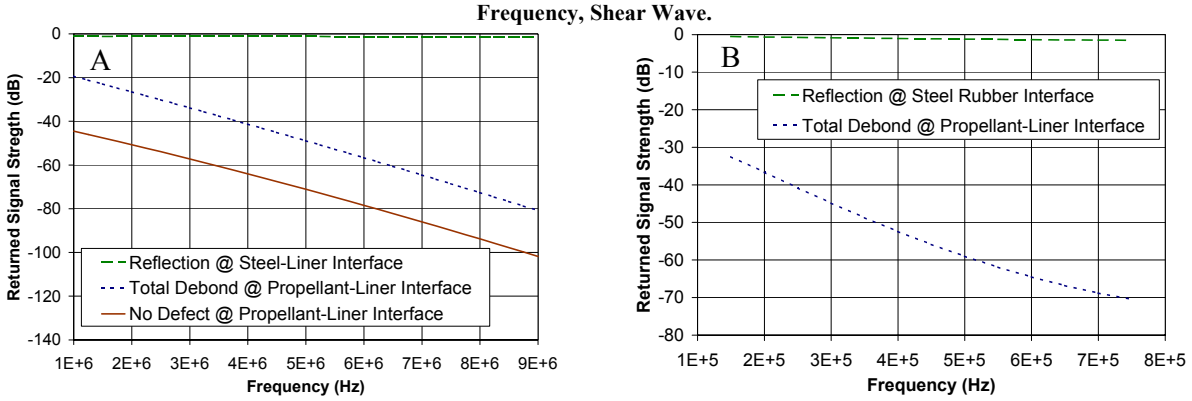

In order to perform an ultrasonic inspection of various bondline conditions, tests were first performed on carefully prepared flat specimens with well-defined bondline conditions. Three flat specimens were fabricated. These would represent complete debond at the rubber-steel interface, complete debond at the rubber-propellant interface, and an intact bond line. The supplied motor specimen contained artificial defects as described earlier in this section. The three flat specimens corresponded to the "Debond Steel", "Debond Rubber", and "general area" of the rocket motor specimen, respectively. Next, similar tests were performed on a motor specimen.

Figure 6-A shows the corresponding responses for the flat specimens in the frequency domain. This was calculated using the whole waveform record, such that the series of echoes had enough time to completely subside. The frequency spectrum of the reflected waveforms is also dominated by the casing's front face echo. If the casing had a larger thickness, or if one could use a transducer with higher frequency, one could remove the front face echo from the time domain, as this echo would be completely separated from the subsequent echoes. It was decided not to attempt such removal of the front wall echo, since the exact point in time where one would cut off the time domain response could substantially affect the outcome.

Figure 6: (A) Frequency domain representation of longitudinal wave inspection on flat specimen. (B) Deviation of the frequency responses of intact bond and propellant/liner debond from that of the bare steel.

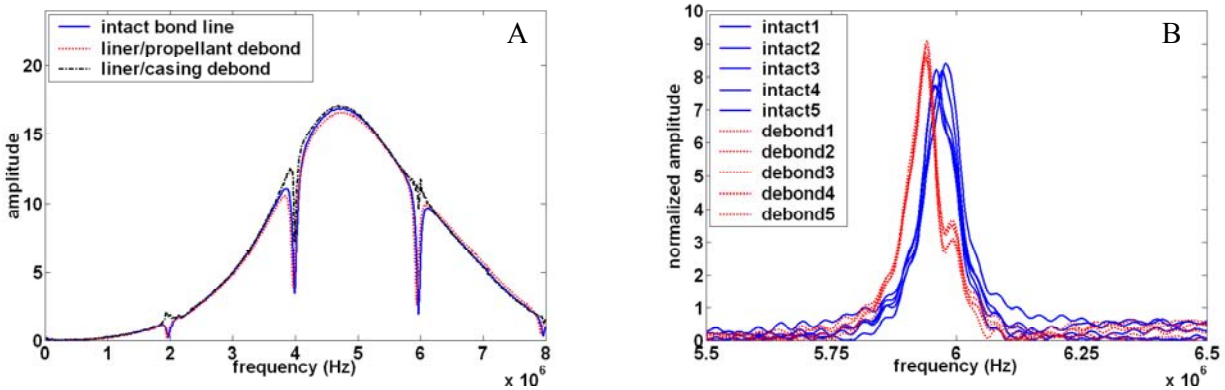

Alternatively, one could de-convolve the responses of an intact bond and debond at the fuel-rubber interface using that of the steel case (debond at the steel-rubber interface) as a reference. This would be equivalent to taking a transfer function approach. One should be able to detect the contributions of the liner and propellant to the total signal, provided that the signal-to-noise ratio is adequate in the frequency domain responses. The drawback to this proposed technique is the

drop in the signal-to-noise ratio in the resonant areas of the spectrum as well as in the area away from the ultrasonic probe's center frequency.

To work around this drawback, it was decided to simply subtract the magnitude spectrum of the steel plate from those of the "intact bond" and "debond fuel" as plotted in Figure 6-B for the 6 MHz region. This showed small shifts in the resonance frequencies and a small difference in magnitudes at all frequencies. In order to assess the significance of these observed differences, five individual data sets were collected from randomly selected inspection locations. It can be seen that the variation in spectrum magnitudes between bonded and debonded data sets at non-resonant frequencies is not significant. In contrast, the plots at the resonant frequencies cluster into two separate groups and hence the difference is statistically significant, although very small.

Figure 7: (A) Frequency domain representation of longitudinal wave inspection on rocket specimen. (B) Deviation of the frequency responses of intact bond and propellant/liner debond from that of the steel/rubber debond.

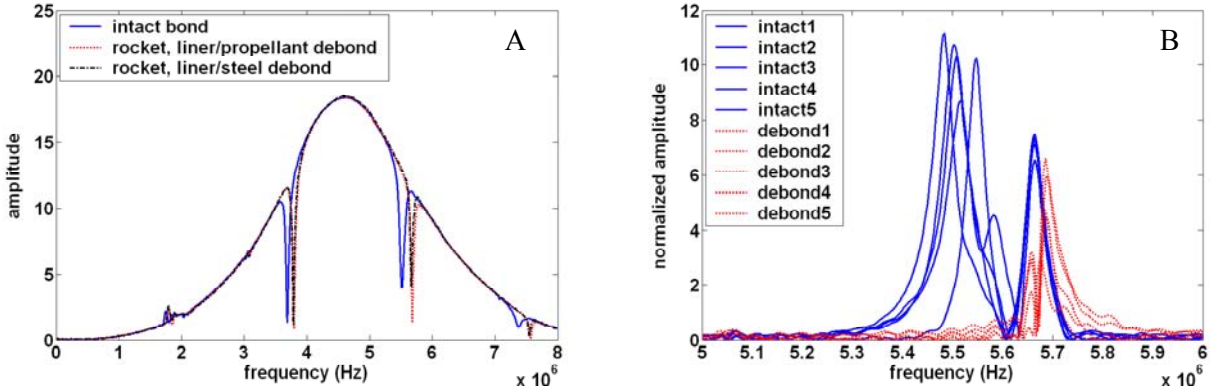

The same normal beam compression wave tests were performed on the rocket specimen, which produced similar results as presented in Figure 7. The shift in resonant frequency is more pronounced than seen previously for the flat samples. The larger shift in resonant frequency resulted in the double peak in the difference spectrum of Figure 7-B.

Discussion: It is evident from Figure 5-A and Figure 5-B that the signal received from the defect is many orders of magnitude smaller than that received from the interface between the steel case and the liner. It is also clear that at high frequencies (6.5 MHz for longitudinal, and 500 kHz for shear) the signal loss exceeds 60 dB. These two factors, combined with the relative thinness of the layers comprising the motor structure (steel case 1.58 mm, rubber liner 1.88 mm) impose contradictory constraints. The low magnitude ratio between the rubber/propellant echo signal and the casing/rubber echo mandates the use of very high frequencies to achieve maximum time resolution; otherwise, the former signal will be lost in the latter. Conversely, the extreme attenuation necessitates the use of very low frequencies (where the time resolution is poor) to receive the strongest possible defect signal. The contradictory constraints are even worse for shear waves, which are desirable for the detection of kissing bonds. These constraints are seen to disqualify methods such as those suggested by [9], which rely on time-domain inspection.

Figure 5-A and Figure 5-B have grave implications for the use of guided Lamb waves, which have a strong shearing component [16]. The shear losses are so high, that a frequency ceiling of the order of 100 kHz must be set. However, this will lead to wavelengths that are too large for inspection of such a thin layer. In addition, the large impedance mismatch would force almost all of the wave energy into the steel casing, where there is almost no sensitivity to the rubber/propellant interface. This limits the usefulness of Lamb wave techniques as an inspection tool in this case. It was decided therefore to use frequency-domain resonance techniques here.

It could be argued that a small change in the thickness of the steel plate could result in a similar frequency shift in the resonant frequencies. A thickness difference of 0.007 mm between steel plates that was used in the fabrication of specimens would correspond to the observed shift at 6 MHz. However, the plates were ground at the same machining pass together and the variation in

their thickness was less than 0.005mm. Moreover, a variation in local thicknesses of the test spots would manifest in similar scatter patterns in the intact and debond cases of Figure 6-B. However, it is obvious that the intact bond case shows a larger scatter at the resonant frequency. This could be attributed to the presence of composite solid propellant, which is more susceptible to local inhomogeneity.

Similar to the flat specimens, one could argue that the difference in resonance frequencies of the two cases shown in Figure 7-B could merely be a result of variation in the local casing thickness. A thickness difference of 0.055 mm would correspond to such a shift in the frequency domain. This should be outside the casing thickness variation that one would expect for a rocket casing.

Conclusions: The frequency dependant shear and longitudinal wave velocities and attenuation coefficients of the rubber liner material used in a solid propellant rocket motor were measured. These, in conjunction with the properties of the other components of the motor were used to characterize the ultrasonic response of the layered motor structure. The vast impedance difference between the rocket casing and rubber liner and the high attenuation coefficient of the rubber makes it extremely difficult to get ultrasonic energy into the liner and then back again into the casing. In particular, the enormous shear wave attenuation coefficient prevents the application of Lamb wave-based techniques.

Normal beam compression wave testing is the only realistic method of interrogating the rubber/propellant interface, although such wave modes are not well-known for sensitivity to kissing bonds. Total debonds are detectable by this technique, although the relevant signatures are not very strong and require great care in test setup for obtaining reproducible results. Such indications of debonds were observed in the frequency domain on flat plate samples. The damaged areas of an analog rocket motor with artificial defects were also detectable by ultrasound. Any further work in this area should make a thorough assessment of the effects of casing thickness and the protective paint layer on the detection sensitivity.

The authors wish to acknowledge the financial support provided by Defence Research and Development Canada, and project oversight of Dr. Franklin Wong at DRDC Valcartier.

References:

1. Viktorov, I.A., Rayleigh and Lamb Waves, Plenum Press, New York (1967).
2. Brekhovskikh, L.M., Waves in Layered Media, 2nd edition, Academic Press, New York (1980).
3. Lynnworth, L.C., Ultrasonic Measurement of Elastic Moduli in Slender Specimens Using Extensional and Torsional Wave Pulses", Journal of Testing and Evaluation, Vol. 1, No. 2, 119-125 (1979).
4. Freemantle, R.J. and Challis, R. E., "Combined Compression and Shear Wave Ultrasonic Measurements on Curing Adhesive", Measurement Science and Technology, Vol. 9, 1291-1302 (1998).
5. Bar-Cohen, Y., Mal, A.K., and Yin, C. C.,"Ultrasonic Evaluation of Adhesive Bonding", J. Adhesion, Vol. 29, 257-274 (1989).
6. Billson, D.R. and Hutchins, D. A.,"Laser-EMAT Ultrasonic Measurements of Bonded Metals", Nondestr. Test Eval., Vol. 10, 43-53 (1992).
7. Peter Cawley, "Ultrasonic Measurements for the Quantitative NDE of Adhesive Joints – Potential and Challenges", 1992 IEEE Ultrasonics Symposium, pp 767-772 (1992).
8. Guy, P., Jungman, A., and Nayfeh, H., "Assessment of Bond Quality Between Metal Components", Review of Progress in Quantitative NDE, Vol. 11B, 1355-1361 (1992).
9. P. Gammell 1993 IEEE Ultrasonics Symposium pp. 659-661 (1993).
10. Madaras, E., Winfree, W., Smith, B.T. and Heyman, J.H., Detection of Bondline Delaminations in Multilayer Structures with Lossy Components, NASA-CR-182716 (1988).
11. Sachse, W. and Pao, Y.H.,J. Appl. Phys. 49(8):4320 (1978).
12. Lee, C.C., Lahham, M., and Martin, B.G., IEEE Trans. Ultrason., Ferroelectr., Freq. Contr. 37(4), 286 (1990).

13. O'Donnell, M., Jaynes, E.T., and Miller, J.G., J. Acoust. Soc. Am., 69(3), 696 (1981).
14. Newell, K. J., Sinclair, A.N., Fan,Y. and Georgescu, C., Res. Nondestr. Eval 9:25-39 (1997).
15. Levesque, D., Hebert, H., and Monchalin, J., Ultrasonic Determination of the Elastic Constants of Damaged Propellant, Final Report, National Research Council Canada, Industrial Materials Institute, (1998).
16. Krautkramer. Ultrasonic Testing of Materials. Third Edition, New York: Springer-Verlag, p 620, (1983).